JOURNAL OF SOLID STATE CHEMISTRY 77, 1–14 (1988)

Thermodynamic Stability of Ternary Oxides in *Ln–M*–O (*Ln* = La, Pr, Nd; *M* = Co, Ni, Cu) Systems

A. N. PETROV, V. A. CHEREPANOV, A. YU. ZUYEV,
AND V. M. ZHUKOVSKY

Chemistry Department, Urals State University, Lenin Avenue 51,
Sverdlovsk, 620083, USSR

Received February 23, 1988

The phase equilibria in *Ln–M*–O systems (*Ln* = La, Pr, Nd; *M* = Co, Ni, Cu) were investigated in the temperature range 937–1573 K and for oxygen partial pressures of 10^{-15}–1 atm. The boundaries of the stability of the single phases were determined by emf techniques using 0.9 ZrO_2 + 0.1 Y_2O_3 as the solid-state electrolyte. Based on these data the thermodynamic properties of single phases were calculated. The different cross sections of *Ln–M*–O phase diagrams are presented.

Introduction

The ternary oxides of rare-earth and 3*d*-transition metals form an important and interesting object of study, because of their electrical, magnetic, and catalytic properties.

Phase equilibria in *Ln*–Fe–O systems (*1, 2*) have by now been most thoroughly investigated. With increasing atomic number of the transition metal, a marked complexity arises in the phase relations. At present, information on the ternary rare earth and 3*d*-transitional metal (cobalt, nickel, copper) oxides with the following composition is available: $LnMO_3$, $Ln_4M_3O_{10}$, $Ln_3M_2O_7$, Ln_2MO_4, which some authors (*3, 4*) claim to be related to oxides of a homologous series such as $Ln_{n+1}M_nO_{3n+1}$, $Ln_2M_2O_5$, $LnMO_2$. Without dwelling on the problem of phase relations in detail it is noteworthy that, as yet, there is no consistency in literature as to the composition and the stability regions of ternary oxides.

The successful use of oxide materials is in many respects limited by our knowledge of their thermodynamic stability limits with external variations of temperature and partial oxygen pressure P_{O_2}. Thermodynamic investigations of the systems under review have been neglected until recently. A number of papers on the thermodynamic characteristic of ternary oxides, when examined in detail, proved to be incorrect because of the lack of reliable information on phase equilibria. For example, estimates of the Gibbs energy of formation of $LaCoO_3$ (*5*) and $LaNiO_3$ (*6, 7*) are considered to be incorrect, since in the interpretation of their decomposition the authors failed to take into account the formation of intermediate phases such as $La_4M_3O_{10}$ (*3, 8–12*). Be-

0022-4596/88 $3.00

cause the presence of $LaCuO_2$ (*13*) had not been taken into account, the electrochemical cell emfs were compiled incorrectly in the study of the thermodynamic stability of La_2CuO_4 (*14*). The results of Ref. (*15*) can be considered as satisfactory only in the limited temperature range under investigation, since these authors did take into account the $LaCuO_2$ phase even when it was thermodynamically unstable (below 1180 K).

Sufficiently reliable data, based on the correct phase diagram (*9*) were obtained by the authors (*10*) only for the La–Co–O system within the interval of 1175–1325 K. In our previous papers (*11, 12, 16, 17*) the temperature ranges for La–Co–O and La–Ni–O systems up to 1073–1473 K and for a cobaltate series of rare-earth metals ($LnCoO_3$ where Ln = Sm, Eu, Gd, Tb, Dy, Ho) were increased.

However, in a number of cases the thermodynamic properties of ternary oxides in the Ln–M–O systems (where Ln = La, Pr, Nd; M = Co, Ni, Cu) are still unknown, while in others they are in need of elucidation and the temperature ranges need to be enlarged.

The present paper deals with the thermodynamic stability of ternary oxides on the basis of a phase diagram analysis of Ln–M–O systems using the emf technique in which the solid-state electrolyte ($0.9\ ZrO_2 + 0.1\ Y_2O_3$) has been employed.

Experimental

Thermodynamically stable forms of the rare-earth element oxides (99.9% purity) and 3*d*-transition metal oxides (Co_3O_4, NiO, Cu_2O) of "pure for analysis" and "special purity" qualification were used as starting materials.

The phase relations in the systems under study were ensured by equilibrium sintering of mixtures with the fixed values of composition ξ_{Ln}; ξ_M ($\xi_{Ln} = n_{Ln}/n_{Ln} + n_M$), temperature ($T$, K), oxygen pressure ($P_{O_2}$), within the limits $0.20 \leq \xi_{Ln} \leq 0.90$; $973 \leq T, \text{K} \leq 1573$; $10^{-15} \leq P_{O_2} \leq 0.21$ (atm). Here n_{Ln} and n_M are the number of moles of rare-earth elements and 3*d*-transition metals, respectively. Constant values of temperature and partial oxygen pressure during sintering (from 50 to 300 hr) were maintained automatically with an accuracy of ±1 K and $(\lg P_{O_2}) = \pm 0.02$, respectively. High temperature (up to 1773 K) differential thermal (on derivatograph OD-103, system: F. Paulic, J. Paulic, L. Erdey) and microscopic structural (with the help of catetometer KM-6) methods of analysis of tempered patterns were used, as was the powder X-ray diffraction method. The equilibrium oxygen pressures corresponding to any particular region of the phase diagram Ln–M–O, as well as the thermodynamic properties of ternary oxides formed in the systems were studied using the emf technique in conjunction with oxygen concentration cells with separated gas enclosures. The working electrodes of the cells were the equimolar mixtures of phases, corresponding to the regions of interest in the phase diagrams. Oxygen in air was used as a reference electrode. In the cases when the working electrode contained the $Ln_4M_3O_{10}$, $LnCuO_2$ phases we were faced with sluggish kinetics which greatly increased the equilibration time; reliable, reproducible data were obtained only through a modified technique (*12*), involving variable oxygen pressures of the reference electrode. The modified device has made it possible to maintain the emf of the working cell at zero during the entire duration of the experiment, thus substantially increasing the reliability of the thermodynamic data.

The temperature dependences of the galvanic cells emf's were measured both under heating and cooling conditions. To ensure that equilibrium conditions were reached the stabilized potential of the working electrode (for a number of different constant temperatures) was varied by external polarization. The restoration of the emf value to its initial value made it plausible that the partial oxygen pressure corresponded to the equilibrium conditions. Once the measurements were completed the samples of working electrodes were rapidly cooled and then subjected to powder X-ray diffraction analysis.

Results and Discussion

1. Phase Equilibria

Ln–Co–O systems. Powder X-ray diffraction data of the tempered samples showed that in air and in the temperature range 1073–1773 K only one $Ln\mathrm{CoO}_3$ phase with the perovskite-type structure is formed, with the exception of the La–Co–O system. The $La_4Co_3O_{10}$ phase, synthesized earlier under low oxygen pressures (*8–10*), was obtained in air at 1700 K and at higher temperatures in the composition range $\xi_{La} > 0.5$. This phase can also be obtained at lower temperatures with decreasing P_{O_2}. In the *Ln*–Co–O systems, $La_4Co_3O_{10}$ and for the first time $Pr_4Co_3O_{10}$ and $Nd_4Co_3O_{10}$ were synthesized at 1373 K and at $10^{-4.4}$ atm. The preparation time of the series $Ln_4\mathrm{Co}_3\mathrm{O}_{10}$ significantly increased when passing from lanthanum to neodymium. $La_4Co_3O_{10}$ and $Pr_4Co_3O_{10}$ were obtained as pure phases by sintering for 40 and 100 hr, respectively. We failed to obtain $Nd_4Co_3O_{10}$ in a single-phase form even after 465 hr of continuous sintering (1373 K, $10^{-4.4}$ atm.).

Unlike rhombohedral $La_4Co_3O_{10}$ (*8*), praseodymium and neodymium cobaltates $Ln_4\mathrm{Co}_3\mathrm{O}_{10}$ have tetragonal unit cells with the parameters $a = 5.390 \pm 0.005$ Å, $c = 27.36 \pm 0.04$ Å and $a = 5.387 \pm 0.007$ Å, $c = 27.24 \pm 0.07$ Å, respectively.

The possibility of formation of $Ln_2\mathrm{CoO}_4$ phases with the K_2NiF_4-type structure has been confirmed under more rigid reducing conditions. An example of a typical projection of the phase diagram on the Gibbs triangle is shown in Fig. 1.

Ln–Ni–O systems. The ternary oxides $Ln_2\mathrm{NiO}_4$ and $La_4Ni_3O_{10}$ described earlier (*3, 4, 11, 18, 19*) were obtained in air in the temperature range 1173–1673 K.

An unknown phase, obtained in the PR–Ni–O system at 1173 K, has been reported to be $Pr_4Ni_3O_{10}$. However, we were not able to obtain this strictly single phase even under sintering for a period of over 500 hr, because the decrease of temperature led to a deceleration of the solid-state reaction. An increase of temperature led to the decomposition of that phase to Pr_2NiO_4. Nevertheless, on the assumption that the unknown phase is $Pr_4Ni_3O_{10}$, based on the resemblance of the powder X-ray diffraction patterns to $Ln_4\mathrm{Co}_3\mathrm{O}_{10}$, the parameters of tetragonal unit cell were calculated as $a = 5.414 \pm 0.005$ Å, $c = 27.56 \pm 0.06$ Å.

Attempts to obtain orthonickelates of $Ln\mathrm{NiO}_3$ composition in air were unsuccessful. Mixtures with the composition $\xi_{La} = 0.5$ heated for 80 hr in oxygen (under the conditions described in (*7*)) led to the formation of two phases: $La_4Ni_3O_{10}$ and NiO. Probably, $Ln\mathrm{NiO}_3$ compounds are unstable under the specified conditions and can be obtained only at higher oxygen pressures (*20*).

Nickelates of $Ln_3\mathrm{Ni}_2\mathrm{O}_7$ composition (*4*) were not encountered in systems under the cited range of temperatures and oxygen pressures. This supports the findings of Ref. (*3*), where attempts to obtain $La_3Ni_2O_7$ were also unsuccessful.

The compound $La_4Ni_3O_{10}$ is stable in air below 1485 K; above this temperature it decomposes according to the reaction

$$La_4Ni_3O_{10} = 2La_2NiO_4 + NiO + \tfrac{1}{2}O_2.$$

The decomposition temperature was determined by emf techniques with a solid electrolyte and by thermogravimetry. Small differences in the position of X-ray diffraction lines for $La_4Ni_3O_{10}$ (*3*) and "$La_3Ni_2O_7$" (*4*)

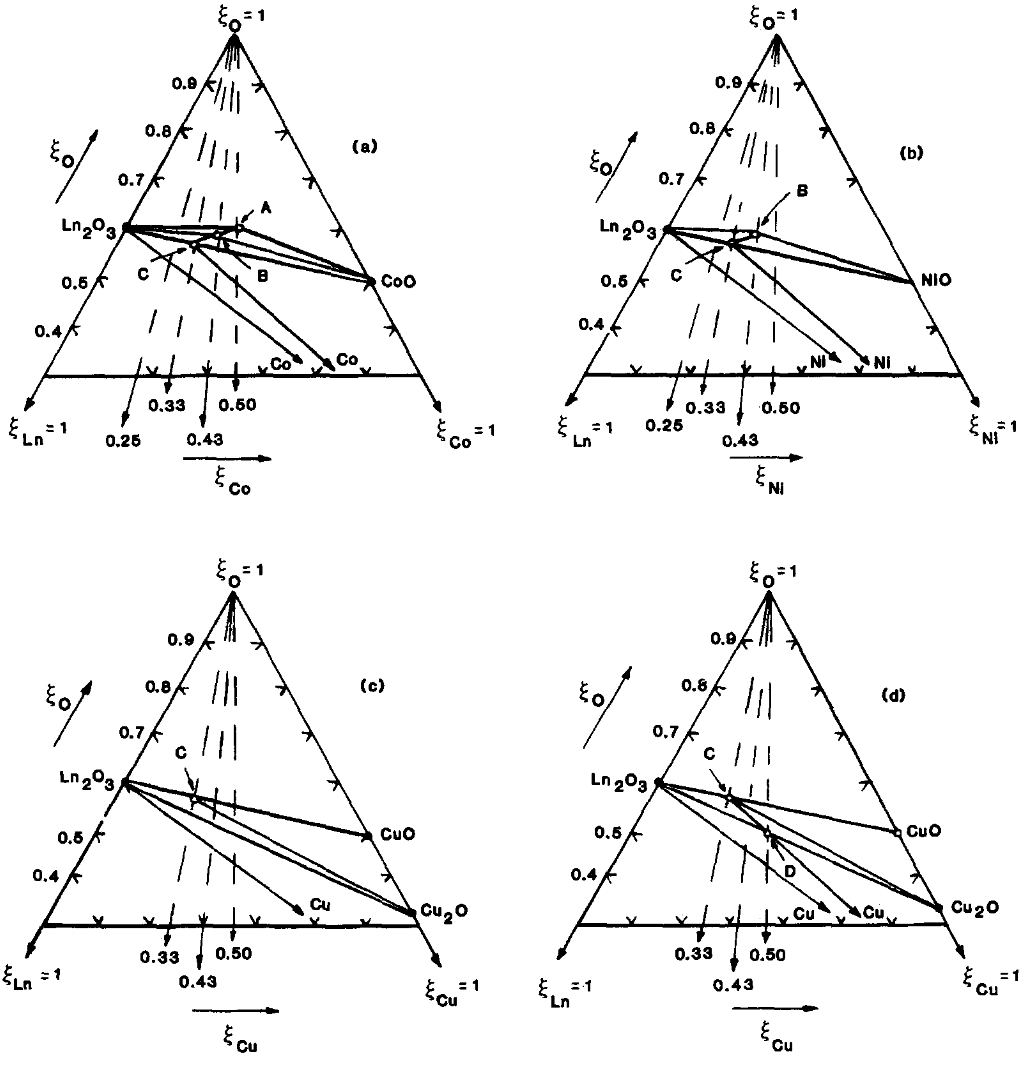

FIG. 1. Phase diagram projection on the Gibbs triangle of composition for the systems (a) *Ln*–Co–O, (b) *Ln*–Ni–O, (c) La–Cu–O ($T < 1180$ K), (d) *Ln*–Cu–O (in the case Ln = La, $T > 1180$ K). Phases: A, $LnMO_3$; B, $Ln_4M_3O_{10}$; C, Ln_2MO_4; D, $LnCuO_2$.

are most probably caused by distortions of one crystal structure caused by oxygen nonstoichiometry, which is a very characteristic feature for this class of compounds.

The typical phase diagram projection on the composition triangle for this system is shown in Fig. 1b.

Ln–Cu–O systems. The ternary oxides Ln_2CuO_4 with the K_2NiF_4-type structure (*21*) were obtained in the *Ln*–Cu–O system in air. $LnCuO_2$ phases with the $CaFeO_2$-type structure (*14*) were synthesized at low oxygen pressures.

Some specific features in the properties of $LaCuO_2$ as compared to the praseodymium and neodymium cuprites of the same composition should be noted. According to the results of homogeneous annealing, La CuO_2 is stable only below 1180 K. That is why phase diagram projections of the La–

Cu–O system on the composition triangle below and above 1180 K are different (Figs. 1c and 1d).

2. *Thermodynamic Studies*

The composition of the working electrodes of electrochemical cells were chosen by taking account of available data on the phase correlations of systems. Oxygen in air was used as the final reference electrode. The various electrochemical cells under study can be presented in the following schematic form.

$$\left.\begin{array}{l} Ln\mathrm{CoO_3},Ln_4\mathrm{Co_3O_{10}},Ln_2\mathrm{O_3},\mathrm{O_2(Pt)}|\mathrm{O^{2-}}|\mathrm{(Pt)O_2} \\ Ln\mathrm{CoO_3},Ln_4\mathrm{Co_3O_{10}},\mathrm{CoO},\mathrm{O_2(Pt)}|\mathrm{O^{2-}}|\mathrm{(Pt)O_2} \end{array}\right\} Ln = \mathrm{La, Pr, Nd} \qquad \begin{array}{r}(\mathrm{I})\\(\mathrm{II})\end{array}$$

$$\left.\begin{array}{l} \mathrm{La_2}M\mathrm{O_4},\mathrm{La_4}M_3\mathrm{O_{10}},\mathrm{La_2O_3},\mathrm{O_2(Pt)}|\mathrm{O^{2-}}|\mathrm{(Pt)O_2} \\ \mathrm{La_2}M\mathrm{O_4},\mathrm{La_4}M_3\mathrm{O_{10}},M\mathrm{O},\mathrm{O_2(Pt)}|\mathrm{O^{2-}}|\mathrm{(Pt)O_2} \\ \mathrm{La_2}M\mathrm{O_4},\mathrm{La_2O_3},M,\mathrm{O_2(Pt)}|\mathrm{O^{2-}}|\mathrm{(Pt)O_2} \end{array}\right\} M = \mathrm{Co, Ni} \qquad \begin{array}{r}(\mathrm{III})\\(\mathrm{IV})\\(\mathrm{V})\end{array}$$

$$\left.\begin{array}{l} Ln_2\mathrm{CuO_4},Ln\mathrm{CuO_2},Ln_2\mathrm{O_3},\mathrm{O_2(Pt)}|\mathrm{O^{2-}}|\mathrm{(Pt)O_2} \\ Ln_2\mathrm{CuO_4},Ln\mathrm{CuO_2},\mathrm{Cu_2O},\mathrm{O_2(Pt)}|\mathrm{O^{2-}}|\mathrm{(Pt)O_2} \end{array}\right\} Ln = \mathrm{La, Pr, Nd} \qquad \begin{array}{r}(\mathrm{VI})\\(\mathrm{VII})\end{array}$$

We have also measured the equilibrium conditions of Co/CoO, Ni/NiO, $\mathrm{Cu_2O/CuO}$ using the following cells.

$$M,M\mathrm{O},\mathrm{O_2(Pt)}|\mathrm{O^{2-}}|\mathrm{(Pt)O_2} \qquad M = \mathrm{Co, Ni} \qquad (\mathrm{VIII})$$

$$\mathrm{Cu_2O,CuO,O_2(Pt)}|\mathrm{O^{2-}}|\mathrm{(Pt)O_2} \qquad (\mathrm{IX})$$

The corresponding reactions are as follows.

$$\left.\begin{array}{l} 2Ln_4\mathrm{Co_3O_{10}} + \tfrac{1}{2}\mathrm{O_2} = 6Ln\mathrm{CoO_3} + Ln_2\mathrm{O_3} \\ Ln_4\mathrm{Co_3O_{10}} + \mathrm{CoO} + \tfrac{1}{2}\mathrm{O_2} = 4Ln\mathrm{CoO_3} \end{array}\right\} Ln = \mathrm{La, Pr, Nd} \qquad \begin{array}{r}(1)\\(2)\end{array}$$

$$\left.\begin{array}{l} 3\mathrm{La_2}M\mathrm{O_4} + \tfrac{1}{2}\mathrm{O_2} = \mathrm{La_4}M_3\mathrm{O_{10}} + \mathrm{La_2O_3} \\ 2\mathrm{La_2}M\mathrm{O_4} + M\mathrm{O} + \tfrac{1}{2}\mathrm{O_2} = \mathrm{La_4}M_3\mathrm{O_{10}} \\ \mathrm{La_2O_3} + M + \tfrac{1}{2}\mathrm{O_2} = \mathrm{La_2}M\mathrm{O_4} \end{array}\right\} M = \mathrm{Co, Ni} \qquad \begin{array}{r}(3)\\(4)\\(5)\end{array}$$

$$\left.\begin{array}{l} 2Ln\mathrm{CuO_2} + Ln_2\mathrm{O_3} + \tfrac{1}{2}\mathrm{O_2} = 2Ln_2\mathrm{CuO_4} \\ 4Ln\mathrm{CuO_2} + \tfrac{1}{2}\mathrm{O_2} = 2Ln_2\mathrm{CuO_4} + \mathrm{Cu_2O} \end{array}\right\} Ln = \mathrm{La, Pr, Nd} \qquad \begin{array}{r}(6)\\(7)\end{array}$$

$$M + \tfrac{1}{2}\mathrm{O_2} = M\mathrm{O} \qquad M = \mathrm{Co, Ni} \qquad (8)$$

$$\mathrm{Cu_2O} + \tfrac{1}{2}\mathrm{O_2} = 2\mathrm{CuO} \qquad (9)$$

On comparing the experimental dependences of temperature vs the emf and the calculated ΔG_T° values of reactions (8 and 9) with reported data (*22–24*) the results were found to be in good agreement. This fact provides ample proof of the proper performance of the cells and the correctness of the data.

The temperature variations of the emfs of cells I–IX are presented in Figs. 2–4. The experimental data were processed using the least-squares method and an M-222 com-

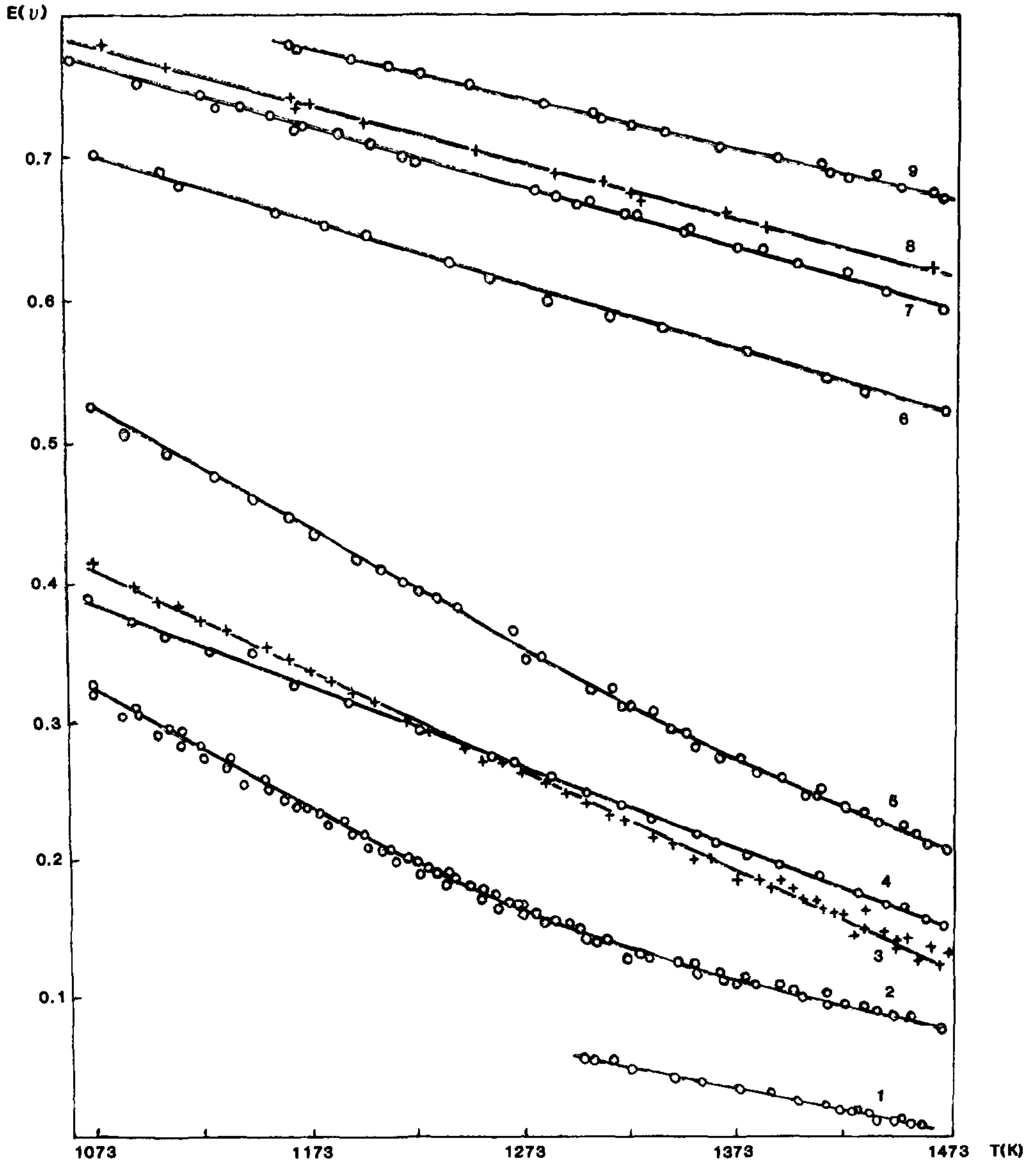

FIG. 2. Electromotive force vs temperature dependences: 1, cell IV (M = Ni); 2, cell I (Ln = La); 3, cell II (Ln = La); 4, cell III (Ln = La, M = Co); 5, cell IV (M = Co); 6, cell VIII (M = Ni); 7, cell V (M = Ni); 8, cell VIII (M = Co); 9, cell V (M = Co).

puter. The coefficients of equations of dependence $E = f(T)$ and the confidence intervals evaluated based on a significance level of random errors of 0.05 are listed in Table I. From the temperature dependences of the emf, the variations of Gibbs standard potential ($\Delta G°$) were calculated with due account for reactions (1–9), as shown in Table II. With the use of ΔG_f° for Ln_2O_3 (*25*) and Cu_2O (*23*) we calculated the changes of Gibbs standard potentials for the process of formation of ternary oxides from the elementary substances (Table III).

Ln–Co–O systems. As compared with

earlier work by Seppanen *et al.* (*10*), the temperature range of our present measurements were substantially widened and the thermodynamic properties of $La_4Co_3O_{10}$ were specified. The breaks in the temperature dependences of the emf of cells I and II at 1205 K are mainly due to first-order phase transition in $LaCoO_3$, which was described in Ref. (*26*).

The thermodynamic properties of the ternary oxides $LnCoO_3$ and $Ln_4Co_3O_{10}$ for *Ln* = Pr, Nd are determined for the first time.

The thermodynamic stability of ternary oxides with Co in the oxidation state 3+ decreases regularly with an increase of the lanthanoid atomic number. The most marked correlation can be found between changes of thermodynamic characteristics of orthocobaltates $LnCoO_3$ and the degree of distortion of their perovskite-type structures. The thermodynamic characteristic $\Delta G°$ of the reaction of formation of $LnCoO_3$ from the binary oxides Ln_2O_3 and CoO is shown for comparison in Fig. 5.

Ln–Ni–O systems. The thermodynamic characteristics of $La_4Ni_3O_{10}$ and La_2NiO_4 are determined in the La–Ni–O system (Table III). On this basis the $\Delta G°(T)$ of reaction (3) has been calculated as

$$\Delta G°(J) = -87600 + 69.39T.$$

Despite the negative Gibbs energy, the oxidation rate of La_2NiO_4 below 1262 K is very slow. Thus, an anneal at 1173 K for 400 hr in air did not yield significant quantities of $La_4Ni_3O_{10}$. The boundary of thermodynamic stability was confirmed by carrying out the opposite reaction in which $La_4 Ni_3O_{10}$ was reduced to La_2NiO in the presence of La_2O_3.

The determination of thermodynamic characteristics of Pr_2NiO_4 and Nd_2NiO_4 by the emf technique is extremely difficult, since the dissociation pressure of these phases is quite close to that of NiO.

Ln–Cu–O systems. With the decrease of temperature, emf curves for cells VI and VII in the La–Cu–O system join at 1183 K.

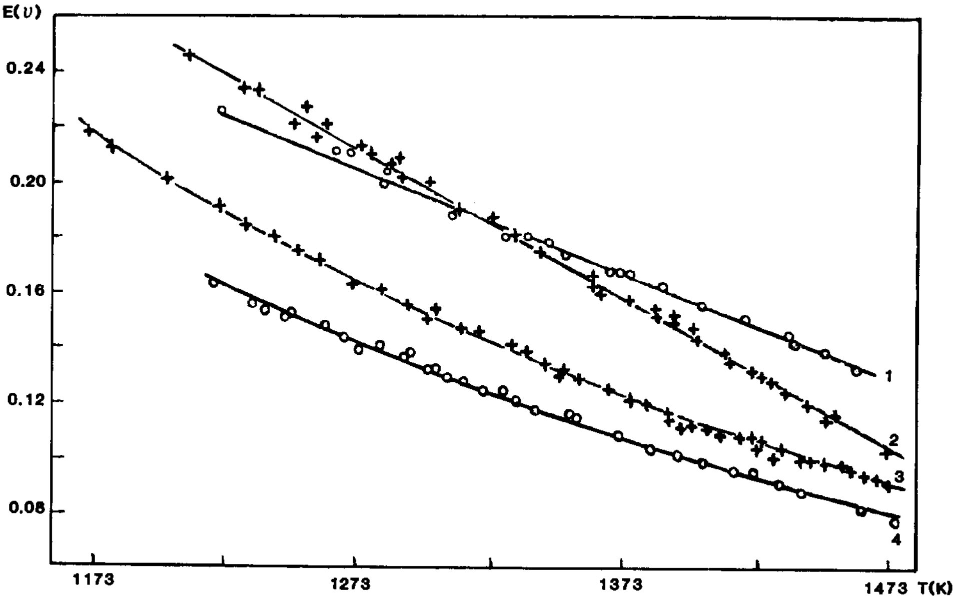

FIG. 3. Electromotive force vs temperature dependences: 1, cell II (*Ln* = Nd); 2, cell II (*Ln* = Pr); 3, cell I (*Ln* = Pr); 4, cell I (*Ln* = Nd).

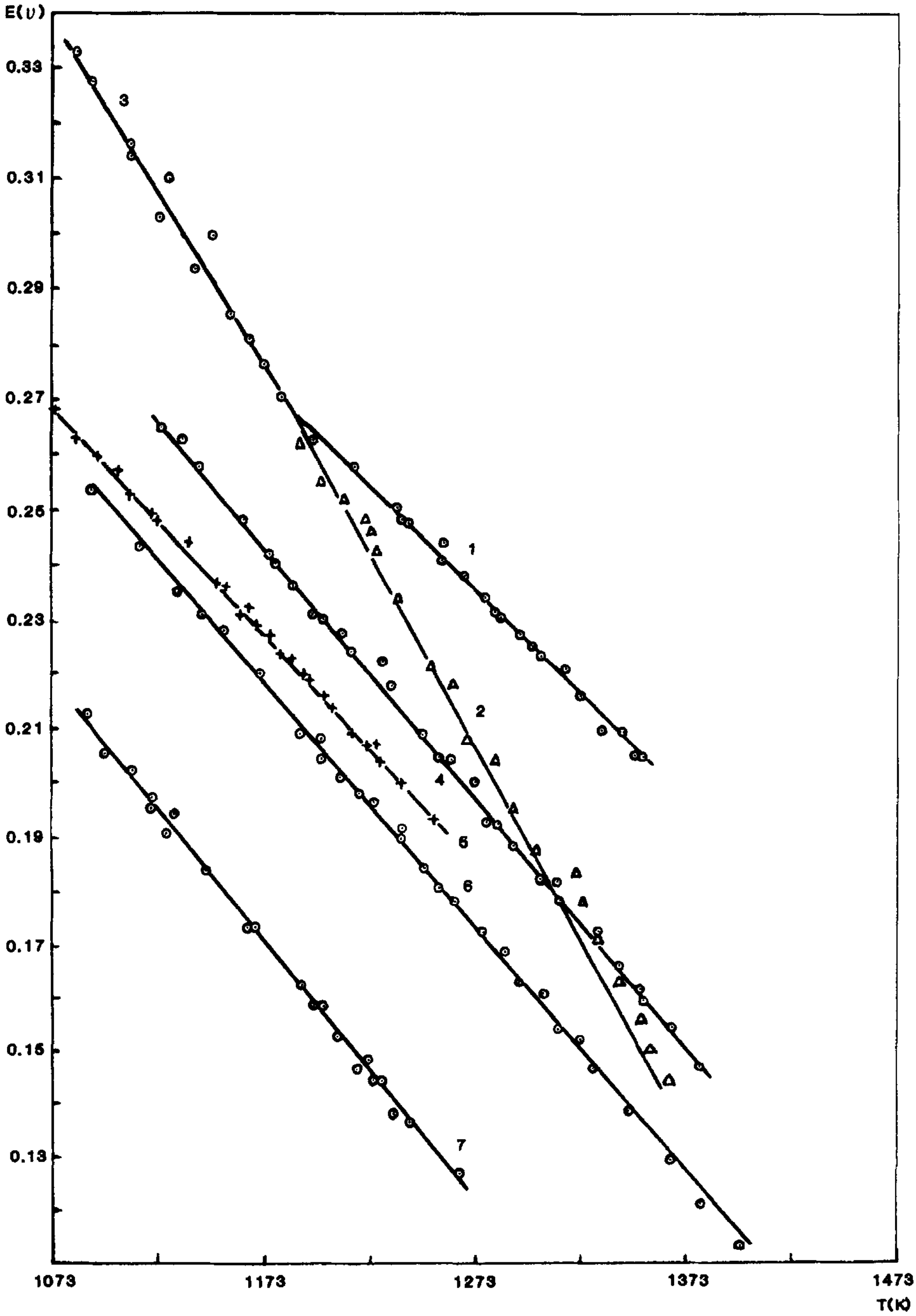

FIG. 4. Electromotive force dependences: 1, cell VI (*Ln* = La); 2, cell VII (*Ln* = La); 3, cell with the working electrode La_2CuO_4, La_2O_3, Cu_2O; 4, cell VI (*Ln* = Pr); 5, cell VII (*Ln* = Pr); 6, cell VI (*Ln* = Nd); 7, cell VII (*Ln* = Nd).

TABLE I

THE RESULTS OF THE STATISTICAL PROCESSING OF THE EMF VS TEMPERATURE DEPENDENCES FOR I–IX CELLS

Cell number	Elements (Ln, M)	Temperature intervals (K)	$E(V) = a + bT + cT^2$			$\Delta E(V) = t_{0.05}S_E[(n)^{-1} + B(T_i - \bar{T})^2]^{1/2}$			
			a	$-b \times 10^4$	$c \times 10^7$	$A \times 10^4$	n	$B \times 10^6$	$\bar{T}$
I	La, Co	1073–1210	1.251	8.65	—	11.80	27	26.14	1139
I	La, Co	1210–1473	2.516	20.88	9.746	8.68	51	1.83	1243
II	La, Co	1073–1213	1.249	7.79	—	42.10	12	51.43	1142
II	La, Co	1213–1473	1.262	8.76	0.711	12.20	34	5.37	1365
III	La, Co	1073–1473	1.005	5.79	—	42.30	23	2.82	1279
IV	La, Co	1072–1473	1.925	16.72	3.435	15.26	54	2.07	1306
V	La, Co	1158–1473	1.190	3.51	—	25.50	20	5.09	1329
I	Pr, Co	1170–1270	0.8461	5.36	—	14.13	12	126.8	1215
I	Pr, Co	1270–1473	1.649	18.53	5.399	31.16	37	3.29	1356
II	Pr, Co	1214–1473	0.9137	5.49	—	45.66	39	4.86	1354
I	Nd, Co	1221–1321	0.6045	3.63	—	26.07	16	68.14	1272
I	Nd, Co	1321–1474	0.8218	7.11	1.396	27.80	17	6.49	1398
II	Nd, Co	1226–1462	0.7117	3.96	—	46.71	21	2.62	1356
IV	La, Ni	1200–1473	0.450	3.03	—	54.5	25	15.2	1394
V	La, Ni	1070–1473	1.218	4.22	—	58.9	26	3.05	1265
V	Nd, Ni	1080–1473	1.135	3.83	—	14.0	33	2.75	1286
VI	La, Cu	1190–1350	0.736	3.94	—	23.7	20	26.9	1276
VII	La, Cu	1190–1380	1.056	6.67	—	59.3	20	16.3	1270
VI	Pr, Cu	1120–1380	0.786	4.64	—	24.0	29	6.6	1245
VII	Pr, Cu	1070–1250	0.717	4.18	—	19.2	27	14.9	1160
VI	Nd, Cu	1110–1380	0.753	4.57	—	22.1	29	5.5	1239
VII	Nd, Cu	1080–1270	0.744	4.90	—	25.0	20	18.2	1172
VIII	Co	1163–1473	1.200	3.94	—	56.40	20	7.50	1331
VIII	Ni	1070–1473	1.221	4.79	—	21.6	15	5.87	1247
IX	Cu	1200–1320	0.619	4.78	—	2.7	6	120	1279

Note. $t_{0.05}$, Student's criterion for the significance level of random errors of 0.05; S_E, identical dispersion of equation $E = f(T)$; n, number of experimental points; $A = t_{0.05}S_E$; $B = \left[\sum_{i=1}^{n} (T_i - \bar{T})^2\right]^{-1}$; $\bar{T} = (n)^{-1} \sum_{i=1}^{n} T_i$.

This leads to the conclusion that the La CuO_2 compound becomes thermodynamically unstable below 1183 K. In this case the chemical mechanism of the potential-forming reactions is altered. The La_2CuO_4, La_2O_3, and Cu_2O phases then coexist under equilibrium conditions. This fact has been confirmed by the results of equilibrium anneals. Therefore, the composition of the working electrodes of cells VI and VII remain unequilibrated until completion of the solid phase-forming processes during transformation of the phases. This, in its turn, leads to a larger spread in emf values of cells at temperatures below 1183 K. For this reason the thermodynamic characteristics of La_2CuO_4 and $LaCuO_2$ were calculated in the range 1183–1400 K. The low value of the upper temperature ranges to which the thermodynamic properties of the *Ln*–Cu–O system were limited are due to the low melting points of the mixtures in those systems.

Phases with composition $LnCuO_2$ (*Ln*

TABLE II

TEMPERATURE DEPENDENCES OF EQUILIBRIUM OXYGEN PRESSURE AND CHANGES OF GIBBS ENERGIES OF POTENTIAL-FORMING REACTIONS

Number of reaction	Elements (Ln, M)	Temperature interval (K)	$lg(P_{O_2}/\mathrm{Pa}) = C + DT + KT^{-1}$			$\Delta G^\circ_T(\mathrm{J}) = A + BT + CT^2$			$\Delta(\Delta G^\circ_T)$ (J)
			C	$D \times 10^3$	$-K \times 10^{-2}$	$-A \times 10^{-3}$	B	$-C \times 10^2$	
1	La, Co	1073–1210	21.76	—	252.16	241.42	160.4	—	90
1	La, Co	1210–1473	66.57	19.64	507.15	485.54	589.4	18.81	60
2	La, Co	1073–1213	20.02	—	251.76	241.0	143.8	—	380
2	La, Co	1213–1473	21.98	1.43	254.38	243.54	162.6	1.37	90
3	La, Co	1073–1473	15.99	—	202.57	193.9	105.2	—	350
4	La, Co	1072–1473	38.02	6.92	388.02	371.5	316.2	6.63	100
5	La, Co	1158–1473	11.39	—	239.86	229.6	61.6	—	220
1	Pr, Co	1170–1270	15.12	—	170.65	163.4	96.9	—	190
1	Pr, Co	1270–1473	41.67	10.88	332.49	318.2	351.1	10.42	160
2	Pr, Co	1214–1473	15.39	—	184.17	176.3	99.5	—	300
1	Nd, Co	1221–1321	11.64	—	121.85	116.6	63.6	—	250
1	Nd, Co	1321–1473	18.65	2.81	165.65	158.6	130.7	2.69	190
2	Nd, Co	1226–1462	12.30	—	143.46	137.3	69.9	—	270
4	La, Ni	1200–1473	10.40	—	90.70	86.8	52.0	—	500
3	La, Ni	1200–1473	11.58	—	91.29				
5	La, Ni	1070–1473	12.80	—	245.00	235.0	75.0	—	300
6	La, Cu	1180–1400	12.26	—	148.32	142.0	69.5	—	200
7	La, Cu	1180–1400	17.74	—	212.87	203.8	122	—	400
6	Pr, Cu	1120–1380	13.66	—	158.76	152.0	82.9	—	100
7	Pr, Cu	1070–1250	12.79	—	145.18	139.0	74.6	—	200
6	Nd, Cu	1110–1380	13.53	—	151.45	145.0	81.7	—	150
7	Nd, Cu	1080–1270	14.17	—	150.00	143.6	87.8	—	260
8	Co	1163–1473	13.26	—	241.88	231.7	69.5	—	290
8	Ni	1070–1473	14.00	—	246.00	235.6	86.0	—	200
9	Cu	1200–1400	13.98	—	124.82	119.5	86.0	—	100

TABLE III

TEMPERATURE DEPENDENCES OF THE STANDARD GIBBS POTENTIALS OF FORMATION OF THE TERNARY OXIDES FROM THE COMMON SUBSTANCES

Ternary oxides	Temperature intervals (K)	$\Delta G^\circ_f(\mathrm{J/mole}) = A + B \times T \times \lg T + C \times T + D \times T^2$				$\Delta(\Delta G^\circ_f)_{\max}$ (J/mole)
		$-A \times 10^{-3}$	$-B$	C	$D \times 10^2$	
$LaCoO_3$	1073–1200	1250	8.8	302.0	—	1.9
	1200–1473	1074	—	34.2	8.0	2.8
$La_4Co_3O_{10}$	1073–1200	4527	35.2	998.2	—	4.1
	1200–1473	3822	—	−95.1	33.5	3.1
La_2CoO_4	1073–1200	2205	17.6	619.6	−6.6	1.7
	1200–1473	2093	—	474.3	−6.6	2.6
$PrCoO_3$	1170–1270	1239	14.1	305.7	—	4.4
	1270–1473	1162	14.1	178.6	5.2	4.3
$Pr_4Co_3O_{10}$	1170–1270	4548	56.5	994.7	—	4.8
	1270–1473	4454	56.5	485.9	20.8	4.7
$NdCoO_3$	1221–1321	1217	12.2	290.5	—	4.4
	1321–1473	1196	12.2	256.9	1.3	4.4
$Nd_4Co_3O_{10}$	1221–1321	4500	58.6	1023	—	4.6
	1321–1473	4416	58.6	888.6	5.4	4.5
$La_4Ni_3O_{10}$	1300–1473	4159.7	—	675.1	—	3.0
La_2NiO_4	1084–1473	1918.6	—	268.5	—	3.0
$LaCuO_2$	1090–1400	894	—	105.9	—	3.0
$PrCuO_2$	1070–1320	1002.2	−14.13	224.9	—	4.4
$NdCuO_2$	1080–1270	990.4	−12.16	215.3	—	4.5
La_2CuO_4	1090–1400	1818.6	—	246.7	—	3.0
Pr_2CuO_4	1070–1320	2003.3	−28.26	460.7	—	4.4
Nd_2CuO_4	1080–1270	1982.1	−24.33	448.2	—	4.5

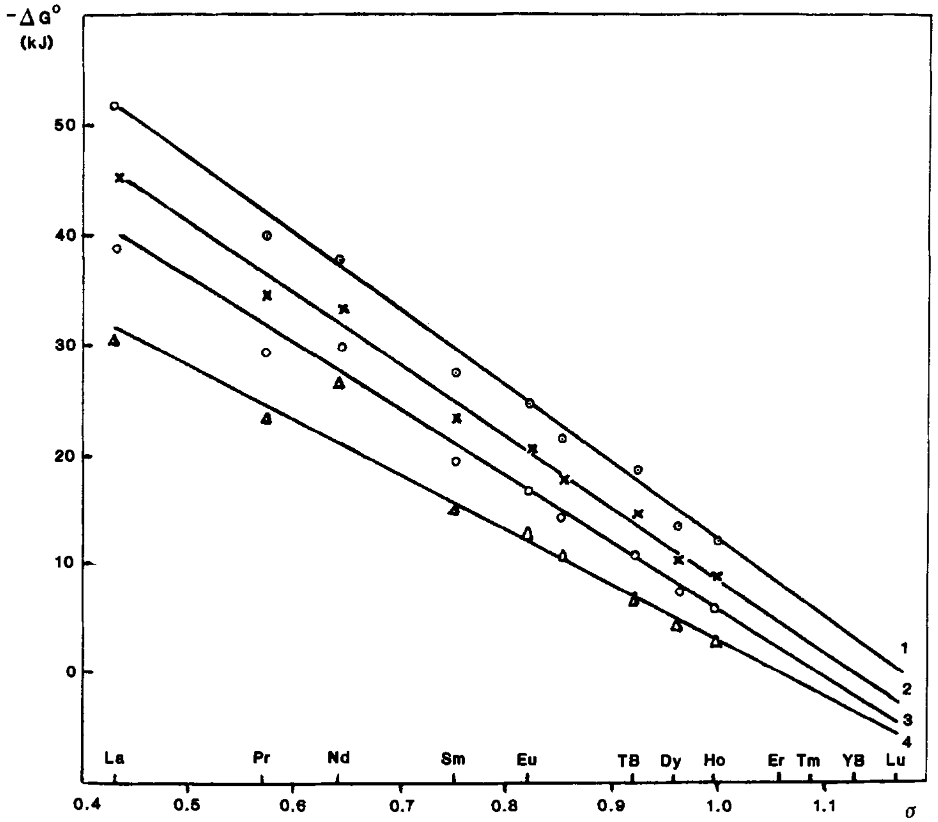

FIG. 5. The formation energy of rare-earth cobaltates from oxides according to the reaction $\frac{1}{2}Ln_2O_3$ + CoO + $\frac{1}{4}O_2$ = $LnCoO_3$ and degree of distortion of the perovskite structure at 1073 K (1), 1173 K (2), 1273 K (3), 1373 K (4).

= Pr, Nd) are stable in all temperature intervals under study. Equilibrium anneals at low P_{O_2} have shown that $LnCuO_2$ phases decompose in the lower range of stability according to the reaction:

$$2LnCuO_2 = Ln_2O_3 + 2Cu + \tfrac{1}{2}O_2. \quad (10)$$

By using reference data for Ln_2O_3 (*25*) the standard Gibbs energy of reaction (10) has been calculated:

$$G^\circ(\mathrm{J}) = 104{,}400\text{–}18.1\,T(\pm 300)\ Ln = \mathrm{La}\qquad 1183 \le T,\ \mathrm{K} \le 1342$$

$$G^\circ(\mathrm{J}) = 178{,}800\text{–}79.5\,T(\pm 350)\ Ln = \mathrm{Pr}\qquad 1123 \le T,\ \mathrm{K} \le 1250$$

$$G^\circ(\mathrm{J}) = 167{,}700\text{–}64.7\,T(\pm 500)\ Ln = \mathrm{Nd}\qquad 1112 \le T,\ \mathrm{K} \le 1263$$

From these dependences the equations for phase boundaries for $LnCuO_2$ were obtained.

$$\lg(P_{O_2}/\mathrm{Pa}) = 6.90 - 10{,}904/T\ (\pm 0.03)\qquad Ln = \mathrm{La}$$

$$\lg(P_{O_2}/\mathrm{Pa}) = 13.30 - 18{,}686/T\ (\pm 0.04)\qquad Ln = \mathrm{Pr}$$

$$\lg(P_{O_2}/\mathrm{Pa}) = 11.76 - 17{,}527/T\ (\pm 0.05)\qquad Ln = \mathrm{Nd}$$

Conclusion

The phase equilibria of nine ternary Ln–M–O-like systems where Ln = La, Pr, Nd; M = Co, Ni, Cu were studied. The thermodynamic characteristics of ternary oxides

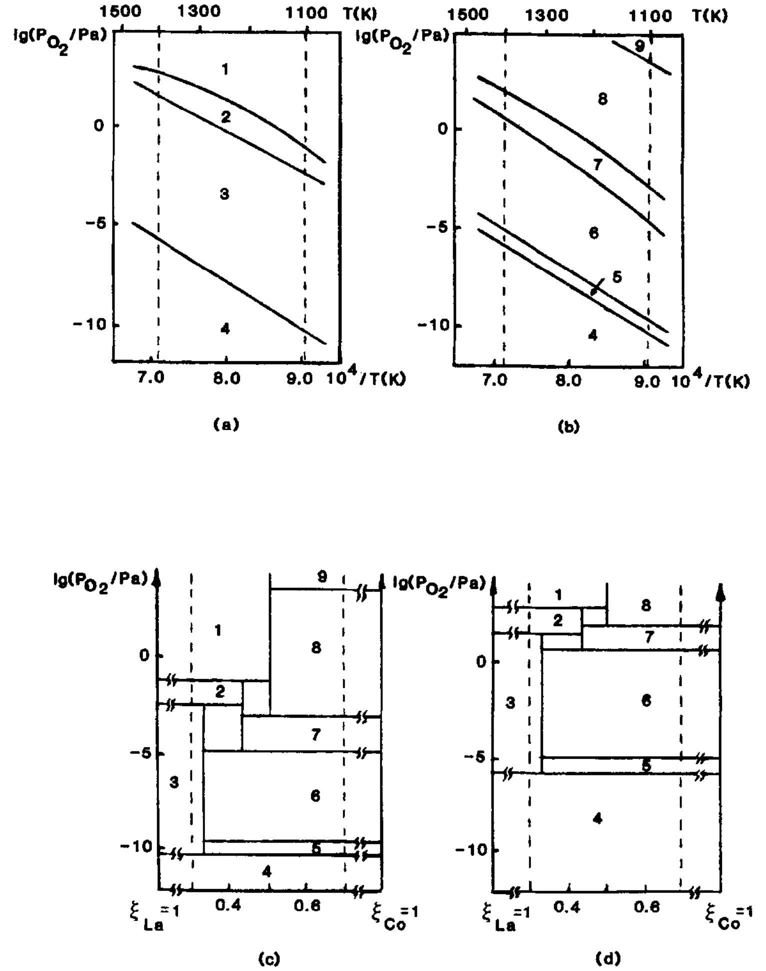

(a) (b)

(c) (d)

FIG. 6. Special cross section of La–Co–O system phase diagram isoconcentrational (a) for $\xi_{Co} = 0.3$; (b) for $\xi_{Co} = 0.7$) and isothermal (c) at 1100 K, (d) at 1400 K). Two-phase regions: 1, La_2O_3, $LaCoO_3$; 2, $La_3Co_3O_{10}$, La_2O_3; 3, La_2CoO_4, La_2O_4, La_2O_3; 4, La_2O_3, Co; 5, La_2CoO_4, Co; 6, La_2CoO_4, CoO; 7, $La_4Co_3O_{10}$, CoO; 8, $LaCoO_3$ CoO, 9, $LaCoO_3$, Co_3O_4.

that delineate the regions of stability with variations of temperature and pressure were obtained. The experimental results permit construction of the phase diagrams of the systems under discussion in different coordinates. Figure 6 illustrates isoconcentrational ($\xi_{Co} = 0.3$ and 0.7) and isothermal ($T = 1100$ and 1400 K) cross sections of the La–Co–O phase diagram. The three-dimensional aspect of the same diagram at 1400 K is given in Fig. 7 as a prism, the base of which forms the Gibbs triangle (see Fig. 1). The horizontal terraces correspond to the equilibria of the three solid phases and are in keeping with observed partial pressure values (see Figs. 6b and 6d). The vertical planes depict two-phase regions of the diagrams, the intersections of lines identify the individual phases in Fig. 7: $LaCoO_3$(A); $La_4Co_3O_{10}$(B), and La_2CoO_4(C). Any phase relations of composite oxide systems *Ln*–*M*–O represented by a set of dots may be regarded as an example of one system of flat and volume-filling geometric figures.

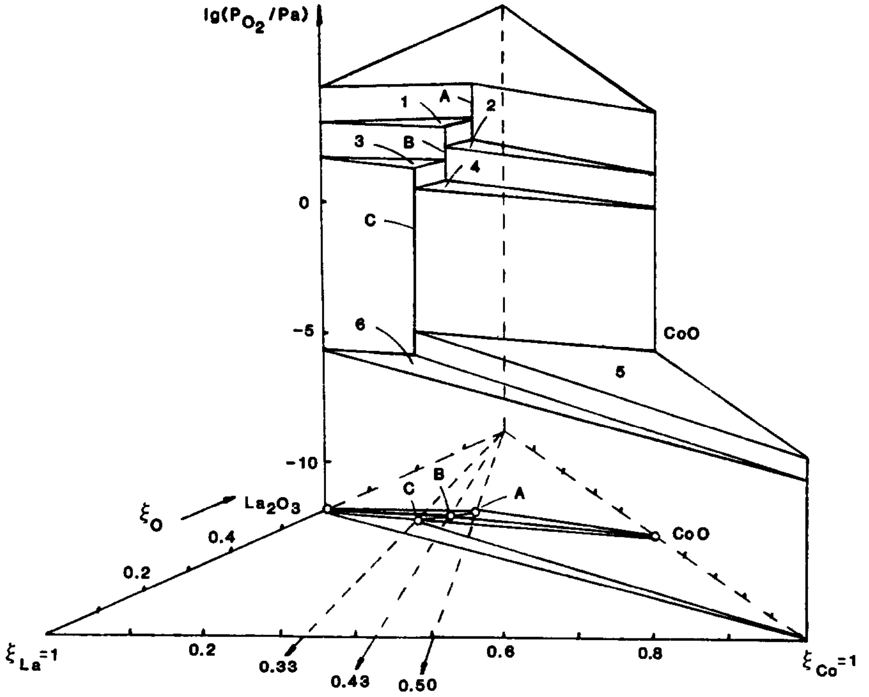

FIG. 7. The phase diagram of the La–Co–O system at 1400 K. Equilibrium oxygen pressure values ($\lg P_{O_2}$/Pa) of the three-phase regions: 2.85 (1), 1.81 (2), 1.52 (3), 0.62 (4), −4.02 (5), −5.74 (6).

Analyses of the thermodynamic stability of the rare-earth and 3*d*-transition metals in the Fe–Co–Ni–Cu set reveal their tendency to form phases of 3*d* metals with a lower oxidation state. This tendency holds also for the simple 3*d* metal oxides. Within one class of ternary oxides, e.g., $LnCoO_3$ and Ln_2CuO_4, the thermodynamic stability decreases with an increase of the rare-earth element number.

References

1. T. KATSURA, T. SEKINE, K. KITAYAMA, T. SUGINARA, AND H. KIMIZUKA, *J. Solid State Chem.* **23,** 43 (1978).
2. H. KIMIZUKA, A. YAMAMOTO, H. OHASHI, T. SIGIHARA, AND T. SEKINE, *J. Solid State Chem.* **49,** 65 (1983).
3. M. SEPPANEN, *Scand. J. Metall.* **8,** 191 (1979).
4. I. DRENNAN, C. P. TAVARES, AND B. C. H. STEEL, *Mater. Res. Bull.* **17,** 621 (1982).
5. O. M. SREEDHARAN AND M. S. CHANDRASEKHARAIAH, *Mater. Res. Bull.* **7,** 1135 (1972).
6. O. M. SREEDHARAN, M. S. CHANDRASEKHARAIAH, AND M. D. KARKHANAVALA, *High Temp. Sci.* **8,** 179 (1976).
7. T. NAKAMURA, G. PETZOW, AND L. GAUCKLER, *Mater. Res. Bull.* **14,** 649 (1979).
8. M. SEPPANEN AND M. H. TIKKANEN, *Acta Chem. Scand. A* **30,** 389 (1976).
9. Y. I. JANECEK AND G. P. WIRTZ, *J. Amer. Ceram. Soc.* **61,** 242 (1978).
10. M. SEPPANEN, M. KYTO, AND P. TASKINEN, *Scand. J. Metall.* **8,** 199 (1979).
11. V. A. CHEREPANOV, A. N. PETROV, L. YU. GRIMOVA, AND E. M. NOVITSKY, *Zh. Fiz. Khim.* **57,** 859 (1983).
12. A. N. PETROV, V. A. CHEREPANOV, E. M. NOVITSKY, AND V. M. ZHUKOVSKY, *Zh. Fiz. Khim.* **58,** 2662 (1984).
13. H. HAAS AND E. KORDES, *Z. Kristallogr.* **129,** 259 (1969).
14. YU. D. TRETYAKOV, A. R. KAUL, AND N. V. MAKUHIN, *J. Solid State Chem.* **17,** 183 (1976).
15. M. S. CHANDRASEKHARAIAH, M. D. KARKHANAVALA, AND O. M. SREEDHARAN, *High Temp. Sci.* **11,** 65 (1979).

16. A. Yu. Kropanev and A. N. Petrov, *Izv. Akad. Nauk SSSR, Neorgan. Mat.* **19,** 2027 (1983).
17. A. N. Petrov, A. Yu. Kropanev, and V. M. Zhukovsky, *Zh. Fiz. Khim.* **58,** 50 (1984).
18. A. Rabenau and P. Eckerlin, *Acta Crystallogr.* **11,** 304 (1958).
19. A. Wold, B. Post, and E. Banks, *J. Amer. Chem. Soc.* **79,** 4911 (1957).
20. G. Demazeau, A. Marbeuf, M. Pouchard, and P. Hagenmuller, *J. Solid State Chem.* **3,** 582 (1971).
21. J. M. Longo and P. M. Raccah, *J. Solid State Chem.* **6,** 526 (1973).
22. E. Jacobsson and E. Rosen, *Scand. J. Metall.* **10,** 39 (1981).
23. O. M. Sreedharan, M. S. Chandrasekharaiah, and M. D. Karkhanavala, *High Temp. Sci.* **9,** 109 (1977).
24. W. G. Bugden and J. N. Pratt, *Trans. Inst. Min. Metall.* **79,** 221 (1970).
25. S. P. Gordienko, B. V. Fenochka, and G. Sh. Viksman, "Termodinamika soedinenii lantanoidov. Naukova dumka," Chap. 9, Kiev (1979).
26. P. M. Raccah and J. B. Goodenough *Phys. Rev.* **155,** 932 (1967).